Multi-Gigabit Interactive Extended Reality over Millimeter-Wave: An End-to-End System Approach

Jakob Struye
IDLab - Department of Computer Science
University of Antwerp - imec
Antwerp, Belgium
jakob.struye@uantwerpen.be

Filip Lemic
i2Cat Foundation
Barcelona, Spain
filip.lemic@i2cat.net

Jeroen Famaey
IDLab - Department of Computer Science
University of Antwerp - imec
Antwerp, Belgium
jeroen.famaey@uantwerpen.be

Abstract—Achieving high-quality wireless interactive Extended Reality (XR) will require multi-gigabit throughput at extremely low latency. The Millimeter-Wave (mmWave) communication bands, between 24 and 300 GHz, can achieve such extreme performance. However, maintaining a consistently high Quality of Experience with highly mobile users is challenging, as mmWave communications are inherently directional. In this work, we present and evaluate an end-to-end approach to such a mmWave-based mobile XR system. We perform a highly realistic simulation of the system, incorporating accurate XR data traffic, detailed mmWave propagation models and actual user motion. We evaluate the impact of the beamforming strategy and frequency on the overall performance. In addition, we provide the first system-level evaluation of the CoVRage algorithm, a proactive and spatially aware user-side beamforming approach designed specifically for highly mobile XR environments.

I. Introduction

From a networking perspective, interactive Extended Reality (XR) is by far the most challenging branch of XR to achieve a consistently high Quality of Experience (QoE) in. As its content is generated in real-time, timely delivery requires extremely high throughput and low latency. The most well-known application is gaming [1], [2], with other applications, such as tele-operation and remote presence (e.g., meetings) also emerging [3]. Wireless interactive XR is expected to benefit from wireless communications in the Millimeter-Wave (mmWave) range, comprising 24 to 300 GHz, as lower frequencies cannot fulfill the multi-gigabit throughput requirements [4]. However, utilizing these frequencies comes with a set of challenges. Most notably, the path and penetration losses of wireless signals scale with the frequency, making establishing high-quality links with mmWave significantly more challenging than with legacy sub-6 GHz solutions. The main mitigation technique is *beamforming*, meaning energy is directionally focused towards a peer, enabling high-gain links with a modest overall energy budget. This is especially challenging in an XR scenario, as these directions change rapidly with highly mobile users. Furthermore, overhead periods dedicated to control communications are in the order of milliseconds with mmWave, making their impact on timely delivery of real-time traffic, such as XR content, non-negligible [5].

While mmWave-based XR systems have frequently been proposed and evaluated over the past years, uncertainty about the upper performance limits in multi-gigabit, high-mobility deployments remains. In theory, mmWave Wi-Fi can offer up to 8 Gbps with a single channel and physical path, but the fluctuating link quality along with the bursty nature and extremely strict latency requirements of the traffic, make multi-gigabit systems challenging to achieve in practice [5].

In this work, we therefore present and evaluate an end-to-end system approach for high-QoE mmWave-based interactive mobile XR. Our system uses IEEE 802.11ay, the most recent mmWave amendment to the Wi-Fi specification, and is evaluated through a simulation of the full networking stack. The simulation further includes highly realistic signal propagation through ray-tracing, realistic XR data streams and real-world user motion traces. Through an extensive set of experiments, we show how a 7 Gbps XR stream can be delivered at high reliability to a highly mobile user. Achieving this does necessitate rapid beamforming at the user-side, as angles of arrival change rapidly during rapid rotational motion. To this end, we integrated the CoVRage algorithm, allowing for proactive beamforming based on predicted rotations, as presented in our previous work [6].

Overall, this work presents the following contributions:

- An end-to-end system approach to interactive XR over mmWave, targeting consistently high QoE for highly mobile users
- A simulation-based analysis of the system's performance, incorporating realistic traffic patterns, real-world 6 Degrees of Freedom (6DoF) user motion, multi-gigabit data rates, highly realistic channel and protocol behavior and metrics representative of actual XR performance.
- Open-source extensions to the IEEE 802.11ay module for the `ns-3` network simulator, including extensions to beamforming functionality and a codebook generator.
- The first full-system evaluation of CoVRage, highlighting its advantages.

The remainder of this paper is structured as follows. Sections II and III provide an overview of IEEE 802.11's mmWave functionality and of related work on mmWave XR evaluations. Section IV contains an overview of the system. Then, Sections V and VI present the simulation experiments and their results, with Section VII concluding this paper.

II. Background

Given the immense requirements wireless interactive XR places on the network, solutions using the common sub-6 GHz bands are not expected to provide sufficiently high performance, given their ubiquitous usage along with limited bandwidth, leading to high congestion. As such, mmWave communications, comprising 24 to 300 GHz is considered a necessity for achieving high-QoE future interactive XR.

A. Millimeter-Wave

The two main current wireless communications standards, IEEE 802.11 and 5G, each provide dedicated mmWave functionality. IEEE 802.11's two mmWave-focused amendments, IEEE 802.11ad and the more recent upgrade IEEE 802.11ay, are especially focused on extremely-high-performance indoors communications, making this technology an ideal fit for indoors wireless interactive XR [7]. A large part of the mmWave functionality addresses challenges which are less prevalent in sub-6 GHz bands, stemming from mmWave's inherently high path loss and low penetration capabilities. To ensure sufficient signal strength over even modest distances, energy must be focused in some intended direction through a process called *beamforming* [8]. To achieve this, mmWave devices are equipped with *antenna arrays*, in which each element transmits or receives a signal with a different phase shift applied to it. Given a carefully selected set of these phase shifts, called an Antenna Weight Vector (AWV), signals will phase-align and therefore interfere constructively in this intended direction. To determine an appropriate AWV, *codebooks* are often used. These define a number of *sectors*, each having an AWV for communications in a different direction. By exhaustively testing every sector in a *sector sweep*, the one providing the highest signal strength can be found. The mmWave Wi-Fi specification defines two processes for AWV selection: the Sector-Level Sweep (SLS) and the Beam Refinement Phase (BRP). During the SLS, which allows for initial association, one side will iterate through all its sectors while the other side deploys a *quasi-omni* AWV, which aims to have a similar signal strength in all directions. Once completed, the two sides switch roles. Then, the BRP allows for further optimization of the AWV through multiple mechanisms, some optional to implement. As beamforming can occur both when transmitting and when receiving, the nodes choose whether to train either their transmit or their receive AWV during the SLS. Commonly, both will train their transmit AWV then, as receive AWV training can be postponed until the BRP.

MmWave Wi-Fi provides a dedicated period for Access Point (AP) discovery and association in its schedule, shown in Fig. 1. Once every Beacon Interval (BI) (102.4 ms by default), a Beacon Header Interval (BHI) period is scheduled. The BHI starts with a Beacon Transmission Interval (BTI), during which the AP transmits a *beacon* on each of its sectors iteratively, informing nodes of its existence and capabilities. If nodes receive these beacons using their quasi-omni AWV, this doubles as the first half of the SLS. The second half can then be performed during the next sub-phase of the BHI, the
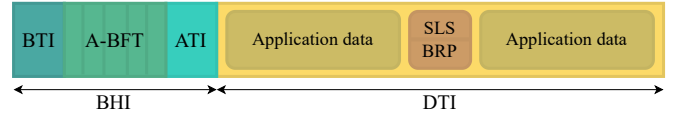

Fig. 1. The Beacon Interval

Association - Beamforming Training (A-BFT). This consists of several *slots* during which nodes can choose to initiate the second half of the SLS. Following a successful SLS, a follow-up BRP may be scheduled either within that A-BFT, or as part of the Data Transmission Interval (DTI), the phase following the BHI. Repeat SLSs with already associated nodes, for example when node mobility threatens to degrade a link, can also be scheduled in this DTI. The DTI is intended mainly for application-level traffic, but parts of it can be reserved for beamforming overhead when needed. In contrast, no application-level traffic may be scheduled during the BHI, which occurs at the start of every BI regardless of current demand for beamforming.

B. CoVRage

Beamforming as described above is an inherently reactive process. In high-mobility scenarios, such as wireless interactive XR, where a user's instantaneous rotational speed may reach hundreds of degrees per second [9], this does not suffice to maintain a stable wireless link. Rotational motion can cause rapid beam misalignment, with occasional beamforming not being responsive enough to adapt in time. To alleviate this, we introduced the Head-Mounted Device (HMD)-side *CoVRage* beamforming algorithm in our previous work [6]. Bypassing the sector-based system entirely, CoVRage leverages modern HMDs' capabilities of accurately estimating their own current pose, as well as predict near-future poses, to synthesize irregularly shaped beams that will consistently offer high gain towards the AP during an expected upcoming rotation. The algorithm was thoroughly evaluated through PHY-level simulations, but was not yet integrated and evaluated as part of an end-to-end XR system.

III. Related Work

Some evaluations of XR over mmWave have been performed, with the performance of the networking aspect being simulated, modelled analytically, or measured empirically using experimental or off-the-shelf hardware. One work investigates the user capacity of such a system with users requiring up to 45 Mbps, through a proprietary 5G simulator [10]. Another work transmits real 3D video and incorporates measured 6DoF user motion into an `ns-3` simulation using the mmWave Wi-Fi module and quasi-deterministic channel model, reporting a high-level metric on user immersion fidelity [11]. In an evaluation on the value of mobile edge computing, the packet latency is reported using the 5G module for `ns-3` [12]. While the appropriate video tiles to transmit were selected based on head rotations, it is unclear if these rotations were also considered within the network simulation. The
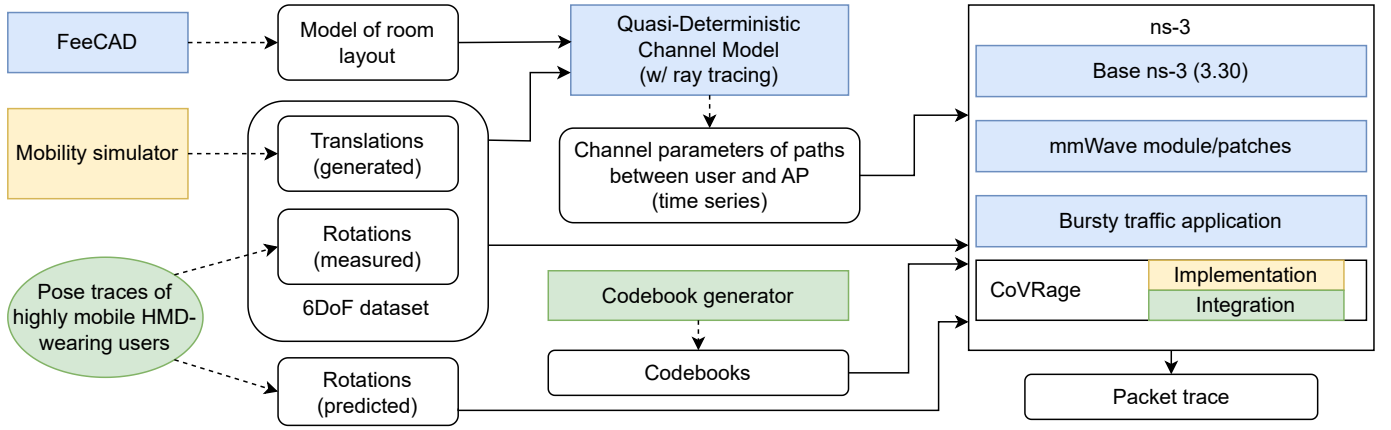
Fig. 2. Overview of the simulation's components. Rectangles denote software, rounded rectangles denote datasets, and ovals denote user experiments. Blue indicates existing open-source software which remained largely unaltered, yellow indicates software by this paper's authors previously presented in other work, and green indicates new software (or experiments) implemented (or performed) especially for this work. All datasets were gathered for this work specifically.

next work compares IEEE 802.11ay link-level throughput with both `ns-3` and real hardware, finding the two to be similar [13]. Similarly, another work compares raw, UDP and TCP throughputs as a function of distance for both the `ns-3` 5G module and IEEE 802.11ad-enabled laptops, with the two again being similar [14]. Another work compares low-level performance of older IEEE802.11ad dongles to a simple, custom simulation model [15]. In terms of hardware-only evaluations, one work investigates throughput reduction caused by mobility-induced blockage when transmitting XR content using off-the-shelf IEEE 802.11ad routers [16]. One final work presents a detailed model encompassing user mobility, XR traffic patterns, channel behavior, transmission schedules and signalling overheads [7]. They report per-packet losses for different maximal latencies and throughputs (max. 200 Mbps).

Overall, none of the existing works cover all the functionality we incorporate into our system, outlined in our contributions in Section I.

IV. END-TO-END MOBILE XR SYSTEM

In this work, we present and evaluate a full end-to-end wireless mobile XR system. We present its design, alongside its implementation in simulation.

A. Design

The interactive XR system is deployed in a large room, with a central ceiling-mounted IEEE 802.11ad AP covering a mobile user. The user has full 6DoF mobility, and receives video frames from the AP at a fixed rate. The AP uses a planar antenna array, capable of 3D beamforming. Through SLS beamforming scheduled in either the A-BFT or DTI, the beam selection from the AP's codebook is kept up to date. For user-side beamforming, the HMD is also equipped with a planar array, and CoVRage is integrated into it. As such, the HMD does not require an explicit codebook for its antenna array, apart from one quasi-omnidirectional AWV.

B. Implementation

In this subsection, we provide details on the different simulation components for the system evaluation, with an overview in Fig 2.

1) Network: The `ns-3` discrete-event simulator handles network simulation. It simulates the wireless network from the physical up to the application layers, allowing for highly realistic simulation. Given `ns-3`'s modular nature, its functionality is easily extended. We use an existing module for IEEE 802.11ad and IEEE802.11ay support [17], [18]. In addition, as part of this work, we developed a number of `ns-3` extensions, all made available to the community[1]. Specifically, we provide the following:

- **CoVRage** [6]: we integrated CoVRage into `ns-3`, maintaining compliance with the Wi-Fi specification. To this end, we equip the HMD with a codebook containing a single directional sector. Whenever CoVRage is executed, its output AWV overwrites the previous AWV of the single sector, both for sending and receiving.
- **Retrain in A-BFT**: in the module, SLS periods for beamforming with previously associated clients can only be scheduled in the DTI. In our patch, such an SLS can be scheduled during the A-BFT as well. This is more efficient from a scheduling perspective, as this period is already reserved for beamforming.

Furthermore, we integrate an additional traffic-generating application [19] into this release of `ns-3`, as the simulator does not come with any traffic generators closely mimicking XR traffic by default. On a configurable interval, this application generates an immediate data burst of a configurable size. This is the type of traffic expected with interactive XR, with each burst corresponding to one video frame.

Furthermore, we use the module in conjunction with a quasi-deterministic channel model in Matlab, enabling highly realistic mmWave propagation based on ray-tracing [20]. We

---

[1]https://github.com/orgs/XR-simulation/repositories

designed a $20 \times 10 \times 10\,\mathrm{m}$ room in FreeCAD and input our own motion patterns (cf. Sec. IV-B3) into the channel model, but did otherwise not modify its code.

2) Codebooks: The `ns-3` module supports a highly realistic codebook format, in which each element's directivity, steering vectors for every (quantized) direction, and full AWV of each sector can be provided through a config file. The module provides some example config files, but no generator for such files. To create our codebooks, we developed such a generator, based on the parser for these files.

One challenging and underexplored aspect of codebook design is the design of the quasi-omni AWV. For this task, we adapted an array synthesis script published by Mathworks [21]. This script finds an AWV using nonlinear optimization. Specifically, the `fmincon` function in Matlab is used to find an AWV which minimizes the objective function $||\mathbf{b_a} - \mathbf{b_t}||_2$, where the vector $\mathbf{b_a}$ denotes the AWV's actual gains for a selection of predefined directions, and $\mathbf{b_t}$ denotes the target gains. The original work samples the gains on a per-degree basis in the azimuthal plane. For this work, we altered the script in several ways, available on this work's GitHub page. Firstly, the objective function was modified to $\max(\mathbf{b_a}) - \min(\mathbf{b_a})$. By aiming to minimize the *range* of gains, we can target a relatively constant gain in all directions without needing to explicitly define a target pattern $\mathbf{b_t}$. Next, we extended the script to support planar arrays, instead of only linear arrays. As this requires evaluation in both azimuth and elevation, rather than only azimuth, we uniformly sample 1000 random azimuth-elevation combinations to determine $\mathbf{b_a}$. Furthermore, as fine-grained per-element amplitude control is not usually implemented in hardware, we restricted the AWV to have fixed amplitudes, with only the phases being variable. With the largest arrays considered in this work, the script's runtime was around one week.

3) User motion: We subdivide the user's 6DoF motion into translational (i.e., walking) and rotational (i.e., turning one's body/head) motion respectively, and take the following approach to obtain these two datasets:

- **Translational motion**: Through our previously published `pm4vr` mobility generator [22], we generate synthetic user mobility paths. The simulator maps virtual paths, within a virtual experience, to physical paths actually walked by users. Through the use of Redirected Walking, users are subtly steered away from walls/obstacles in the physical space without noticeably influencing their intended virtual paths [23]. The simulator generates a simple virtual path, randomly selecting one cardinal direction to move towards every step, then converts this to a physical path. The properties of the physical environment (size, shape, possible obstacles) are easily configured in the simulator, motivating its use.
- **Rotational motion**: As rotational input we simply use real traces of user rotation as measured on a modern HMD. A test subject was asked to perform rotations of varying intensity while wearing a Meta Quest 2 HMD.
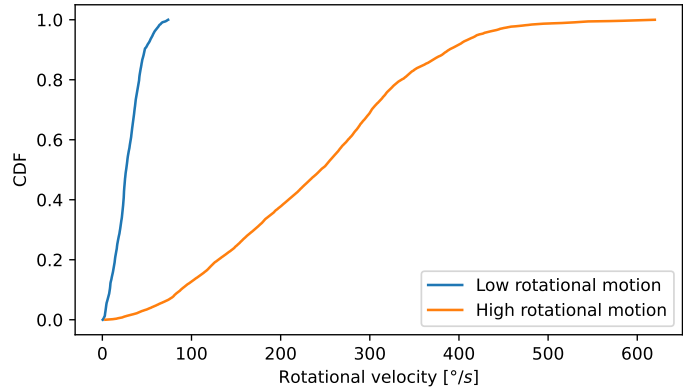

Fig. 3. Rotational velocities, over a 100 ms window.

V. Experiment Design

The simulation experiments presented in this paper are focused on evaluating our end-to-end system, and its sensitivity to several network configuration parameters.

A. Parameters

In each experiment, a user is placed at the center of the room, roaming around in it freely. For rotational motion, we use one of two collected trace files. In the `low` trace, the user was asked to perform slow, steady rotations, while in the `high` trace, the user performed frantic, rapid rotations as much as they were comfortable with while wearing an HMD. Fig. 3 shows their rotational velocities. The application, generating XR-like content, is set to a 100 Hz burst rate (i.e., one burst per 10 ms) and a total data rate of 2, 5, 7 or 8 Gbps (with 8 Gbps being the system's maximum PHY-level data rate). As a baseline for the CoVRage algorithm, the HMD falls back to the regular sector-based system, or uses quasi-omni beams for all communications. When CoVRage is used, upcoming orientations are predicted through either simple constant-velocity extrapolation, or by using the Meta Quest 2's black-box predictor, which was constantly polled while collecting the rotational data traces. As a baseline, an oracle predictor, looking ahead in the trace, is used. The BI is set to either 102.4 ms or 1024 ms. The former allows for more adaptive A-BFT beamforming, while the latter reduces overhead. SLS beamforming, always needed for AP side transmit beamforming, may occur either during the A-BFT or during the DTI. In the first case, it is performed every A-BFT, while in the latter it occurs at a regular interval of once every 100 ms or 1000 ms, being postponed until the start of the next DTI if it is triggered during a BHI. The Modulation and Coding Scheme (MCS) is set to the maximum value of 21. We avoid employing an MCS adaptation algorithm, as these are implementation-dependent, and underestimation of achievable MCS may reduce performance, which would make results more difficult to interpret.

The AP is equipped with an 8×8 antenna array, providing a fair trade-off between signal strength, needed to achieve transmission at high MCS, and beam width, ensuring the

Parameter	Values
Simulation time	20 s
Room size	10×20 m
Rotational motion	Low, **High**
Data rate	2,**5**,7,8 Gbps
Frame rate	100 Hz
RX Beamforming	CoVRage
RX Beamforming (baselines)	Quasi-omni only, sector-based
Motion prediction	Extrapolation, **on-device**
Motion prediction (baseline)	Oracle
BI	**102.4**, 1024 ms
Beamforming timing	in A-BFT, in **DTI**
Beamforming frequency (A-BFT)	once per BI
Beamforming frequency (DTI)	**100**, 1000 ms
AP array size	8×8
HMD array size	8×8 (sectors, quasi-omni)
	64×64 (CoVRage, quasi-omni)

Fig. 4. Latency for CoVRage vs beamforming baselines, 5 Gbps

Fig. 5. Latency for CoVRage vs beamforming baselines, 7 Gbps

user does not leave the beam's range before the AP can adapt. The array's sectors are aimed towards azimuths and elevations from the set $\{-50°, -30°, -10°, 10°, 30°, 50°\}$ with 36 sectors covering every possible combination. A 37th sector uses the quasi-omni AWV. At the HMD, we deploy a 64×64 array, enabling the CoVRage algorithm. For the sector-based baseline, we reduce this to 8×8, as very large arrays require many sectors, which is incompatible with the SLS system, as its runtime scales linearly in the number of sectors. The quasi-omni baseline is run with each of the two arrays, enabling a fair comparison. Table I summarizes these parameters, with defaults in bold.

Simulation time is limited to 20 s per simulation, keeping the runtime of the hundreds of configurations feasible.

B. Metrics

For a high-QoE XR experience, full video frames need to consistently be delivered on-time. Even a small percentage of partially undelivered video frames can lead to a noticeable degradation in quality. In this work, we consider a video frame to be delivered successfully if and only if all packets comprising it arrive within a deadline of 20 ms. For every successful delivery, we calculate its latency as the time between the video frame being offered to the transmitting application, and its final packet arriving at the receiving application layer. As a primary visualization of the performance, we provide Cumulative Distribution Functions (CDFs) of the video frame latency, from which one can read the percentage of successfully delivered video frames within any latency deadline. For each experiment with nonzero video frame loss, its reliability (i.e., the percentage of video frames fully delivered within 20 ms) is displayed on the plot.

VI. RESULTS AND DISCUSSION

We begin by evaluating the performance of CoVRage compared to the sector and quasi-omni baselines. As Fig. 4 shows, only CoVRage is able to maintain a stable connection, with all video frames arriving within 15 ms, well under the 20 ms
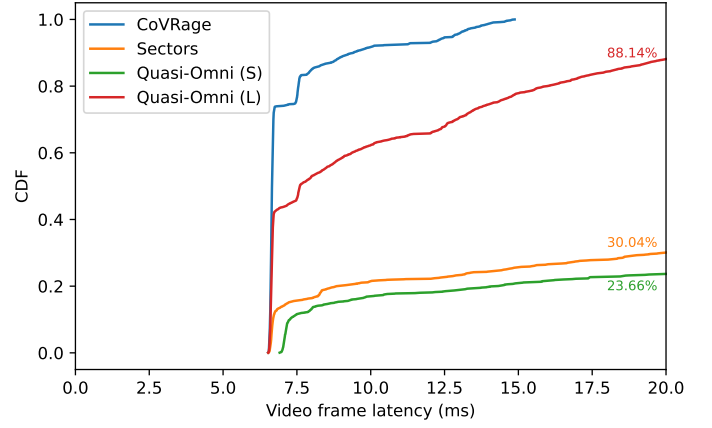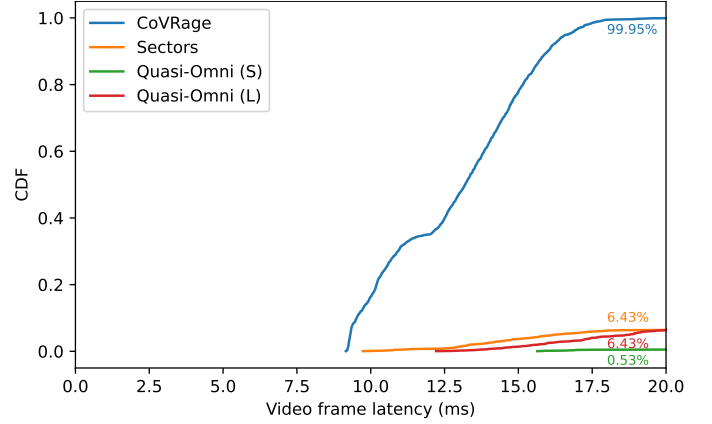
deadline. With the best-performing baseline, namely quasi-omni with a large array, 11.9 % of video frames are lost, while the sector-based and small-array quasi-omni baselines lose 70.0 % and 76.3 % of video frames, respectively. Minimum latency is 6.5 ms, indicating that, under perfect conditions, two-thirds of the 10 ms interval between subsequent video frames is needed to transmit a single video frame. Intuitively, this indicates that the maximal throughput, under ideal conditions, is around 7.5 Gbps. To evaluate this, we repeat the experiment with 7 Gbps in Fig. 5. Here, CoVRage loses only 0.05 %, with baselines losing at least 93.5 %. At 8 Gbps, loss is over 99.8 % in all cases including CoVRage. This is expected, as maximal PHY-level speed is only 8085 Mbps, which is unable to accommodate the 8 Gbps application-layer stream plus overheads from four layers. If we instead reduce the data rate to 2 Gbps, in Fig. 6, losses without CoVRage remain too high for a high-QoE experience.

Next, we investigate the impact of the motion prediction approach on CoVRage, in Fig. 7, at 7 Gbps. Performance is very similar in all three cases, with the on-device prediction nearly matching the oracle, and model-based being very slightly worse. On-device outperforming model-based is expected, as rotation prediction on even decade-old Ocu-
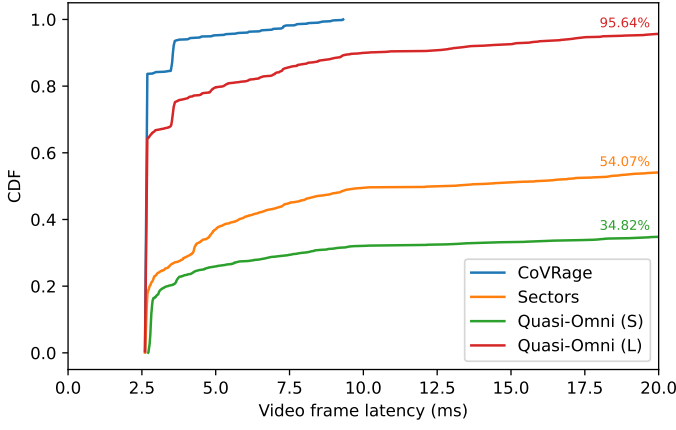
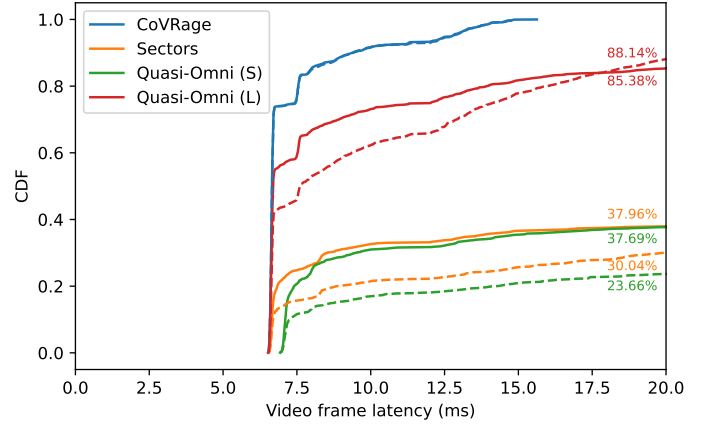Fig. 6. Latency for CoVRage vs beamforming baselines, 2 Gbps
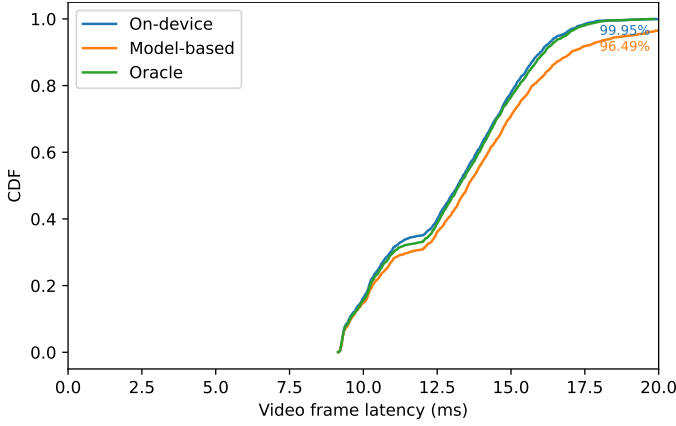

Fig. 7. Latency for CoVRage with different prediction approaches, 7 Gbps

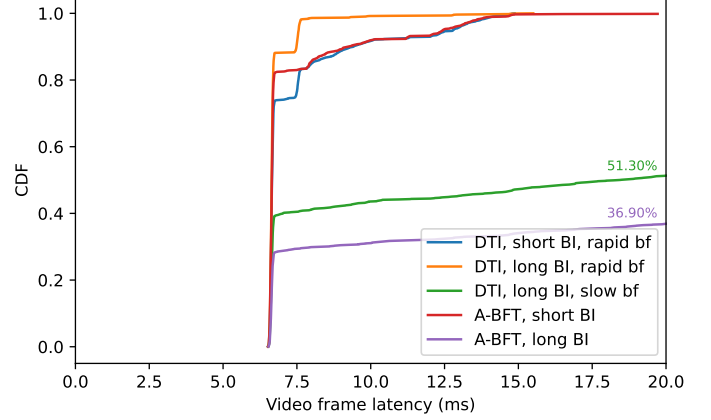Fig. 8. Latency for CoVRage with `low` motion (dashed is `high`), 5 Gbps

Fig. 9. Latency for CoVRage with beamforming in DTI or A-BFT, 102.4 ms ("short") or 1024 ms ("long") BI, beamforming every 100 ms ("rapid") or 1000 ms ("slow") 5 Gbps

lus hardware was based on a constant-acceleration model, which they showed to outperform our simple constant-velocity model [24]. Furthermore, on-device prediction has access to more lower-level sensor readings. It is fair to assume that any modern HMD provides such predictions, as they are needed for content generation. At lower data rates, the differences became nearly imperceptible.

For the next experiment, we repeat the first experiment, but with the `low` motion pattern, in Fig. 8. For the baselines, the intensity of the motion has a clear impact on performance, while for CoVRage the impact is negligible. This shows how CoVRage manages to synthesize effective beams during motion, regardless of motion intensity.

Finally, we investigate the potential of lowering latency by reducing the duration of overhead periods, which do not allow for application data transmission. By default, 10 BIs occur each second, along with 10 SLSs during the DTI. We reduce overhead by reducing the BI frequency by a factor 10, or by moving the SLS to the A-BFT. Note that, when applying both optimizations, the beamforming frequency is also reduced by a factor 10 as an effect. To more thoroughly evaluate the impact of these changes, we also consider the case where DTI beamforming is triggered only once per second. Fig. 9 shows

how rapid beamforming in the DTI combined with a long BI offers the best performance. This is the expected result, as increasing the BI duration reduces the BHI's negative impact on video frame latency. We then compare this scenario to scenarios with a short BI and rapid beamforming, either in DTI or A-BFT. In each case, the long tail of the CDF starts at the 7.6 ms mark, but covers a significantly larger fraction of video frames with a short BI than it does with a long BI. This again makes sense, as 10 times as many BHIs occur with a short BI, making increased latency from waiting for a BHI to finish significantly more likely in these cases. The CDFs for DTI beamforming exhibit a clear plateau between 6.75 and 7.50 ms, mostly absent in case of A-BFT beamforming. This is caused by the SLS, taking 0.75 ms, being scheduled arbitrarily inside the DTI. Apart from this plateau, A-BFT and DTI beamforming perform almost identically at the same interval. Finally, increasing this beamforming interval has a drastic effect on performance, with around half to two thirds of video frames being lost. A user's orientation can change drastically within a second, and more frequent CoVRage beamforming is clearly needed to keep up with these changes. This shows how CoVRage achieves its intended result.

VII. Conclusions and Future Work

In this work, we presented an end-to-end system approach for high-QoE mobile wireless interactive XR using mmWave, evaluating its performance through simulations using realistic input data and channel models. Analyzing a wide array of scenarios revealed that, even at relatively modest data rates and motion patterns, regular beamforming approaches are insufficient to achieve an acceptable QoE. Through rapid head rotations, beams become misaligned before the system has a chance to adapt. When instead utilising the proactive beamforming solution CoVRage, aimed specifically at HMDs, the system was able to consistently deliver a data stream within the 20 ms deadline to the highly mobile user, even at 7 Gbps, near the theoretical throughput limit.

We also identify a number of potential extensions to the system and its evaluation. While the channel model and user mobility already provide a highly realistic single-user environment, real-world deployments are often expected to incorporate several users. This would require the addition of more APs to satisfy the overall data rate need. The potential for spatial sharing is high with mmWave given the directional nature of beams. However, AP assignment and low-latency handovers in such a scenario are challenging, and is the focus of ongoing research. We intend to extend our work with multi-user and multi-AP scenarios, developing solutions to jointly optimize beamforming and AP assignment, as to further assess the feasibility of future wireless XR deployments.

References

[1] A. Hazarika and M. Rahmati, "Towards an evolved immersive experience: Exploring 5G- and beyond-enabled ultra-low-latency communications for augmented and virtual reality," *Sensors*, vol. 23, no. 7, 2023.

[2] S. Gupta, J. Chakareski, and P. Popovski, "mmWave networking and edge computing for scalable 360° video multi-user virtual reality," *IEEE Transactions on Image Processing*, vol. 32, pp. 377–391, 2023.

[3] E. A. Shudayfat, Y. Sharrab, M. Tarawneh, and F. Alzyoud, "Towards virtual university based on virtual reality and terabits internet speed: A review paper," *International Journal of Emerging Technologies in Learning (iJET)*, vol. 17, no. 24, p. pp. 57–68, Dec. 2022.

[4] M. S. Elbamby, C. Perfecto, M. Bennis, and K. Doppler, "Toward low-latency and ultra-reliable virtual reality," *IEEE Network*, vol. 32, no. 2, pp. 78–84, 2018.

[5] J. Struye, F. Lemic, and J. Famaey, "Towards ultra-low-latency mmWave Wi-Fi for multi-user interactive virtual reality," in *GLOBECOM 2020 - 2020 IEEE Global Communications Conference*, 2020, pp. 1–6.

[6] ——, "CoVRage: Millimeter-wave beamforming for mobile interactive virtual reality," *IEEE Transactions on Wireless Communications*, vol. 22, no. 7, pp. 4828–4842, 2023.

[7] J. Morais, S. Braam, R. Litjens, S. Kizhakkekundil, and H. van Den Berg, "Performance modelling and assessment for social VR conference applications in 5G radio networks," in *2021 17th International Conference on Wireless and Mobile Computing, Networking and Communications (WiMob)*, 2021, pp. 225–232.

[8] T. Nitsche, C. Cordeiro, A. B. Flores, E. W. Knightly, E. Perahia, and J. C. Widmer, "IEEE 802.11ad: directional 60 ghz communication for multi-gigabit-per-second Wi-Fi [invited paper]," *IEEE Communications Magazine*, vol. 52, no. 12, pp. 132–141, 2014.

[9] A. Zhou, L. Wu, S. Xu, H. Ma, T. Wei, and X. Zhang, "Following the shadow: Agile 3-D beam-steering for 60 ghz wireless networks," in *IEEE INFOCOM 2018 - IEEE Conference on Computer Communications*, 2018, pp. 2375–2383.

[10] M. Gapeyenko, V. Petrov, S. Paris, A. Marcano, and K. I. Pedersen, "Standardization of extended reality (XR) over 5G and 5G-advanced 3GPP new radio," *IEEE Network*, vol. 37, no. 4, pp. 22–28, 2023.

[11] J. Chakareski, M. Khan, T. Ropitault, and S. Blandino, "6DOF virtual reality dataset and performance evaluation of millimeter wave vs. free-space-optical indoor communications systems for lifelike mobile VR streaming," in *2020 54th Asilomar Conference on Signals, Systems, and Computers*, 2020, pp. 1051–1058.

[12] Y. Liu, J. Liu, A. Argyriou, and S. Ci, "MEC-assisted panoramic VR video streaming over millimeter wave mobile networks," *IEEE Transactions on Multimedia*, vol. 21, no. 5, pp. 1302–1316, 2019.

[13] Z. Wu, C.-Y. Huang, and P. Ramanathan, "Measuring millimeter wave based link bandwidth fluctuations during indoor immersive experience," *IEEE Networking Letters*, vol. 4, no. 3, pp. 113–117, 2022.

[14] K. Zeman, M. Stusek, J. Pokorny, P. Masek, J. Hosek, S. Andreev, P. Dvorak, and R. Josth, "Emerging 5G applications over mmWave: Hands-on assessment of WiGig radios," in *2017 40th International Conference on Telecommunications and Signal Processing (TSP)*, 2017, pp. 86–90.

[15] W. Na, N.-N. Dao, J. Kim, E.-S. Ryu, and S. Cho, "Simulation and measurement: Feasibility study of tactile internet applications for mmWave virtual reality," *ETRI Journal*, vol. 42, no. 2, pp. 163–174, 2020.

[16] J. Struye, H. K. Ravuri, H. Assasa, C. Fiandrino, F. Lemic, J. Widmer, J. Famaey, and M. Torres Vega, "Opportunities and challenges for virtual reality streaming over millimeter-wave: An experimental analysis," in *2022 13th International Conference on Network of the Future (NoF)*, 2022, pp. 1–5.

[17] H. Assasa and J. Widmer, "Implementation and evaluation of a wlan IEEE 802.11ad model in ns-3," in *Proceedings of the 2016 Workshop on Ns-3*, 2016, p. 57–64.

[18] H. Assasa, N. Grosheva, T. Ropitault, S. Blandino, N. Golmie, and J. Widmer, "Implementation and evaluation of a wlan IEEE 802.11ay model in network simulator ns-3," in *Proceedings of the 2021 Workshop on Ns-3*, 2021, p. 9–16.

[19] M. Lecci, A. Zanella, and M. Zorzi, "An ns-3 implementation of a bursty traffic framework for virtual reality sources," in *Proceedings of the 2021 Workshop on Ns-3*, 2021, p. 73–80.

[20] H. Assasa, J. Widmer, T. Ropitault, A. Bodi, and N. Golmie, "High fidelity simulation of IEEE 802.11ad in ns-3 using a quasi-deterministic channel model," in *Proceedings of the 2019 Workshop on Next-Generation Wireless with Ns-3*, 2019, p. 22–25.

[21] R. Gentile, "Array synthesis examples," https://www.mathworks.com/matlabcentral/fileexchange/61588-array-synthesis-examples, Math-Works, January 8 2024, mATLAB Central File Exchange.

[22] F. Lemic, J. Struye, and J. Famaey, "User mobility simulator for full-immersive multiuser virtual reality with redirected walking," in *Proceedings of the 12th ACM Multimedia Systems Conference*, 2021, p. 293–299.

[23] N. C. Nilsson, T. Peck, G. Bruder, E. Hodgson, S. Serafin, M. Whitton, F. Steinicke, and E. S. Rosenberg, "15 years of research on redirected walking in immersive virtual environments," *IEEE Computer Graphics and Applications*, vol. 38, no. 2, pp. 44–56, 2018.

[24] S. M. LaValle, A. Yershova, M. Katsev, and M. Antonov, "Head tracking for the oculus rift," in *2014 IEEE International Conference on Robotics and Automation (ICRA)*, 2014, pp. 187–194.